Copper-and-Nitrogen-Codoped Zirconium Titanate (Cu-N-ZrTiO₄) as a Photocatalyst for Photo-Degradation of Methylene Blue under Visible-Light Irradiation

Lenny Rahmawati[1], Rian Kurniawan[2], Niko Prasetyo[1], Sri Sudiono[1], and Akhmad Syoufian[1*]

[1]Department of Chemistry, Faculty of Mathematics and Natural Sciences, Universitas Gadjah Mada, Sekip Utara, Yogyakarta 55281, Indonesia

[2]Institute of Chemical Technology, Universität Leipzig, Linnéstr. 3, 04103 Leipzig, Germany

Abstract: *Synthesis and characterization of copper-and-nitrogen-codoped zirconium titanate (Cu-N-ZrTiO₄) as a photocatalyst for the degradation of methylene blue (MB) have been conducted. The main purpose of this research was to investigate the co-doping effect of copper and nitrogen dopants in ZrTiO₄ as a photocatalyst for the photodegradation of MB. Titanium-(IV) tetraisopropoxide (TTIP) was dissolved into ethanol and mixed with aqueous zirconia (ZrO₂) suspension containing 10% nitrogen (N) (w/w to Ti) from urea and various amount of copper as dopants. The calcination was performed at temperatures of 500, 700, and 900 °C. The composites were characterized using Fourier transform infrared spectrophotometer (FTIR), X-ray diffractometer (XRD), scanning electron microscopy with energy dispersive X-ray (SEM-EDX) mapping, and specular reflectance UV-Visible spectrophotometer (SRUV-Vis). The degradation of 4 mg L⁻¹ MB solution was conducted for various irradiation times. Characterization shows a significant decrease of the ZrTiO₄ band gap from 3.09 to 2.65 eV, which was given by the composite with the addition of 4% Cu and calcination of 900 °C. Cu-N-ZrTiO₄ composite can degrade MB solution up to 83% after 120 min under the irradiation of visible light.*

Keywords: *band gap; degradation; methylene blue; Cu-N-codoped ZrTiO₄*

■ INTRODUCTION

Dyes are one of the larger groups of pollutants in wastewater from textiles and other industrial processes that can contaminate the environment. Most of the dyes have stable aromatic molecular structures, large molecular sizes, and are difficult to degrade in nature [1]. One of the dyes found in wastewater is methylene blue. Methylene blue ($C_{16}H_{18}N_3SCl$) is a cationic heterocyclic aromatic compound that is used in the textile industry as a dye, but its waste has ecological toxicity and carcinogenicity [2]. Several waste decomposition methods have been developed, such as ozonation, chlorination, and biodegradation. However, these methods have several disadvantages, such as high operational costs and the use of chemical reagents [3]. Therefore, an alternative method is needed for wastewater treatment that can accelerate the decomposition of dye waste. The photo-degradation method is effective for wastewater treatment because it is relatively inexpensive and easy to apply [4].

Degradation of dye waste has become a vital necessity to solve environmental problems and photocatalytic systems have received great attention for the removal of contamination [5]. In the photocatalytic process, light energy is required for the excitation of the photocatalyst. Photocatalyst is a photoactive material that uses photons to catalyze a reaction [6]. In heterogeneous photocatalysis, the photocatalyst is a metal oxide semiconductor with a corresponding band gap energy of about 1.7–3.2 eV [7]. Several semiconductor materials are currently being developed and investigated as photocatalysts, such as Fe_2O_3 [8], CuO [9], ZnO [10], and ZrO_2-TiO_2 [11]. The mechanism of photo-degradation of organic compounds by a photocatalyst is presented in Fig. 1.
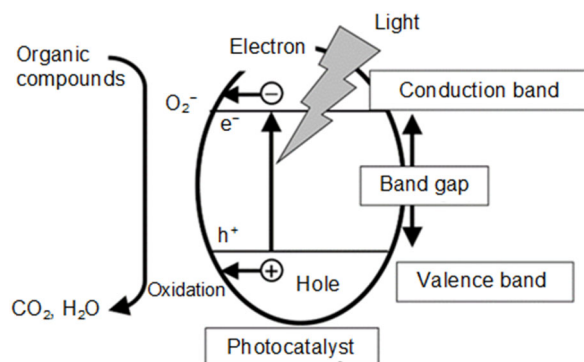
Fig 1. Mechanism of photocatalytic reactions of organic compounds [12]

The reaction can be explained as follows [13].

photocatalyst + hv (photon) $\rightarrow$ h^+ (hole) + e^- (electron)

$e^- + O_2 \rightarrow {}^{\cdot}O_2^-$

$h^+ + OH^- \rightarrow {}^{\cdot}OH$

${}^{\cdot}O_2^- + $ organic compounds $\rightarrow CO_2 + H_2O$
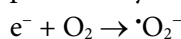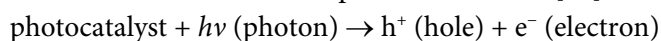
Titanium dioxide (TiO_2) is widely used in photocatalytic reactions because it is non-toxic, stable, and has high efficiency in the degradation of organic pollutants [14]. The three phases of TiO_2 are rutile, anatase, and brookite. Rutile is the most stable phase of TiO_2, anatase is metastable, and brookite will transform to rutile at temperatures above 600 °C [15]. The anatase phase of TiO_2 has a band gap energy of 3.20 eV, while the rutile has 3.02 eV. Although the band gap of anatase (3.20 eV) is slightly higher than rutile (3.02 eV), it exhibits superior photoactivity under UV light irradiation to that of rutile [16]. The degradation of methylene blue by several photocatalysts has been presented in Table 1. Synthesis of TiO_2-S has been reported to degrade methylene blue up to 69.49% under visible light for 300 min of irradiation time [17]. The percentage of degradation of methylene blue by TiO_2 with dopants carbon (C) and nitrogen (N) reached 87% under visible light irradiation [18].

Zirconium dioxide (ZrO_2) is a p-type semiconductor with a wide band gap in the range of 3.25–5.00 eV. ZrO_2 has low thermal conductivity, corrosive resistance, high mechanical, and stable photothermal properties [21]. ZrO_2 has good stability and easily produces holes in the valence band, leading to strong interactions with the active component. ZrO_2 has three

Table 1. Percent degradation of methylene blue by several photocatalysts

Photocatalysts	Percent degradation (%)
TiO_2-S	69.49 [17]
N-codoped TiO_2	87.00 [18]
N-doped TiO_2/ZrO_2	86.30 [19]
ZrO_2-TiO_2	81.20 [20]

polymorphic phases, including cubic (above 2370 °C), tetragonal (1170–2370 °C), and monoclinic (below 1170 °C) [22]. ZrO_2 is active under UV light; therefore, it needs to be modified to increase photocatalytic activity. The way to increase the photocatalytic activity of ZrO_2 is to combine it with a TiO_2 semiconductor. The addition of ZrO_2 to TiO_2 has been reported to increase the stability of anatase more than rutile [23]. ZrO_2 has been known as a support material for TiO_2. The presence of Zr^{4+} in TiO_2 will increase the stability of the anatase at high temperatures (900 °C) [24].

Coupling ZrO_2 with TiO_2 will give the advantages of a large surface area, thermal stability, and resistance to heat and corrosion [25]. Zirconium titanate ($ZrTiO_4$) modified by the doping method will decrease the band gap to visible light. Several studies have reported that doping can be done with metals such as Fe [26], Mn [27], and Zn [28] and also non-metals such as N [29] and C [30]. In this study, copper (Cu) and nitrogen (N) were chosen as dopants because they have good charge-carrier separation efficiency. Nitrogen (N) is one of the elements that is effective in improving the mechanical properties and conductivity of metal oxide ions [31]. Several methods of preparing $ZrTiO_4$ codoped by Cu-N have been reported, such as the template-free hydrothermal method [32] and the polymer complex solution method [33]. Both methods still use toxic organic solvents, which are expensive and not environmentally friendly.

In this research, copper and nitrogen were codoped into $ZrTiO_4$ composite through the simple-and-environmentally-friendly sol-gel process. The goals of this study are to investigate the co-doping effects of metal-nonmetal (Cu and N) on $ZrTiO_4$ composite and its application as a photocatalyst to degrade methylene blue under visible light illumination. Various amounts of copper dopant (2, 4, 6, 8, and 10% (w/w to titanium))

were used to study their performance in shifting the bandgap of nitrogen-doped ZrTiO$_4$. Variation of calcination temperatures (500, 700, and 900 °C) was carried out to study the stability of the crystal structure and its influence on the photocatalytic activity of the composite. Furthermore, photocatalytic evaluation was done by applying Cu-N-ZrTiO$_4$ as a photocatalyst to degrade methylene blue under visible light irradiation for 120 min.

■ EXPERIMENTAL SECTION

Materials

Titanium(IV) tetraisopropoxide (TTIP, 97% purity, Sigma-Aldrich) was used as a TiO$_2$ precursor, and zirconia powder (ZrO$_2$, Jiaozuo Huasu) was used as the coupling metal oxide. Copper(II) sulfate pentahydrate (CuSO$_4$·5H$_2$O, Merck) and urea (Merck) were used as dopant sources. Absolute ethanol (99.5% purity, Merck) and demineralized water (Jaya Sentosa) were used as solvents. Methylene blue (MB) (Thermo Fisher Scientific India Pvt. Ltd.) was used as a dye for the photocatalytic test.

Instrumentation

Fourier transform infrared spectroscopy (FTIR) was done to observe absorption from the range of 400 to 4000 cm^{-1} using the Thermo Nicolet iS10 (Thermo Fisher Scientific, USA). X-ray powder diffractometer (XRD) PANalytical X'Pert PRO MRD (Liaoning, China, Cu Kα radiation λ = 1.54 Å, 40 kV, 30 mA) was used to examine the crystalline structure of the materials. The crystal size (L) was calculated by the Scherrer equation [34],

$$L = \frac{0.9\lambda}{B\cos\theta}$$

where λ is the wavelength of the X-ray, θ is the Bragg angle, and B is half the full width of the maximum intensity of the peak in radians. The morphology of photocatalyst and the presence of copper-nitrogen were observed by scanning electron microscope equipped with an energy dispersive X-ray spectrometer (SEM-EDX) JSM-6510LA (Bridge Tronic Global, USA) and an accelerating voltage of 15 kV. The bandgap was determined from the absorption spectra obtained using specular reflectance UV-Vis spectrometer UV (SR-UV)

1700 Pharmaspec (Shimadzu, Japan). The band gap energy was calculated based on the absorption edge cross method of the absorbance spectra using the photon energy function [35],

$$E_g = \frac{hc}{\lambda}$$

where E$_g$ is the band gap energy (eV), h is Planck's constant (6.62607 × 10^{-34} J/s), c is the speed of light (3 × 10^8 m), and λ is the edge wavelength (nm). Photocatalytic degradation of MB was tested using a LIFE MAX 30W/765 PHILIPS TLD lamp. The concentration of MB solution after degradation was determined by absorption at 664 nm using a Thermo Scientific Genesys 50 UV-Vis Spectrophotometer (Antylia Scientific, US).

Procedure

Synthesis of Cu-N-ZrTiO$_4$

Copper-and-nitrogen-codoped zirconium titanate were prepared by the sol-gel method. Initially, 2.5 mL of TTIP was dissolved in 25 mL of absolute ethanol and then stirred homogeneously. Amount of 1 g of ZrO$_2$ powder and 86.8 mg of urea (10% w/w to Ti) were dispersed into 10 mL of demineralized water along with 30.4, 63.5, 95.2, and 127 mg of CuSO$_4$·5H$_2$O. The copper concentration was varied with a ratio of 2, 4, 6, 8, and 10% (w/w to Ti). The mixture was stirred for 30 min. To separate the precipitate, the suspension was centrifuged at 2000 rpm for 1 h. The precipitate was aged in ambient condition for 24 h and then dried at 80 °C for 24 h. Finally, the composites were calcined at temperatures of 500, 700, and 900 °C for 4 h under atmospheric conditions. All composites were characterized using FTIR, XRD, SEM-EDX, and SRUV-Vis. N-doped ZrTiO$_4$ composite without Cu was also prepared as a reference.

Photocatalytic degradation of methylene blue

Firstly, 15 mg of Cu-N-ZrTiO$_4$ with various concentrations of Cu dopant was dispersed in 30 mL of 4 mg L^{-1} aqueous MB. Under continuous stirring, the mixture was irradiated with a LIFE MAX 30W/765 PHILIPS TLD lamp for 15, 30, 45, 60, 75, 90, 105, and 120 min. The solution was centrifuged for 30 min at

3000 rpm to separate the photocatalyst. The concentration of MB after photocatalytic degradation was determined by absorption at 664 nm. Quantitative analysis of enhanced photocatalytic decomposition of MB was examined by employing a pseudo-first-order kinetic model [36]:

$$-\frac{dC}{dt} = k_{obs}C$$

in which,

$$\ln C = --k_{obs}t + \ln C_0$$

where C is the concentration of MB (mg L^{-1}), t is irradiation time (min), and k$_{obs}$ is the observed rate constant for the photocatalytic decomposition (mg L^{-1} min^{-1}). Plots were given for irradiation time of 0 to 60 min as the highest photoactivity was observed in this time interval.

■ **RESULTS AND DISCUSSION**

FTIR characterization was conducted to determine the functional groups in Cu-N-ZrTiO$_4$. FTIR spectra of 4% Cu-N-ZrTiO$_4$ is shown in Fig. 2. ZrO$_2$ and N-doped ZrTiO$_4$ materials were used as references. The broad absorption band in the range of 500–600 cm^{-1} can be attributed to the stretching vibrations of Ti–O and Cu–O [14]. The peaks at the wavenumber of 512 and 1635 cm^{-1} are associated with the Zr–O and Zr–OH vibrational bands, respectively, which confirm the presence of ZrO$_2$ [21]. The absorption band at about 1120 cm^{-1} increases up to 4% Cu co-doping, which could potentially be associated with Cu–O–Zr or Cu–O–Ti bonds, or both [18]. The peak intensity of ZrO$_2$ at 1600 cm^{-1}, which is H–O–H bending [5], indicates a shift in vibration absorption to 1570 cm^{-1} in N-doped ZrTiO$_4$ due to the formation of N–Ti–O.

The absorption band that appears around 3400 cm^{-1} in all samples is recognized as the O–H stretching vibration of H$_2$O [4]. It comes from the water molecules that are adsorbed during the synthesis process. FTIR spectra of 4% Cu-N-ZrTiO$_4$ calcined at 700 and 900 °C display a weak absorption of Zr–O at 500–600 cm^{-1}. This is due to a phase transformation from anatase to rutile [17]. Absorption bands at 3300–3400 and 1600 cm^{-1} decrease as the calcination temperature increases. The high
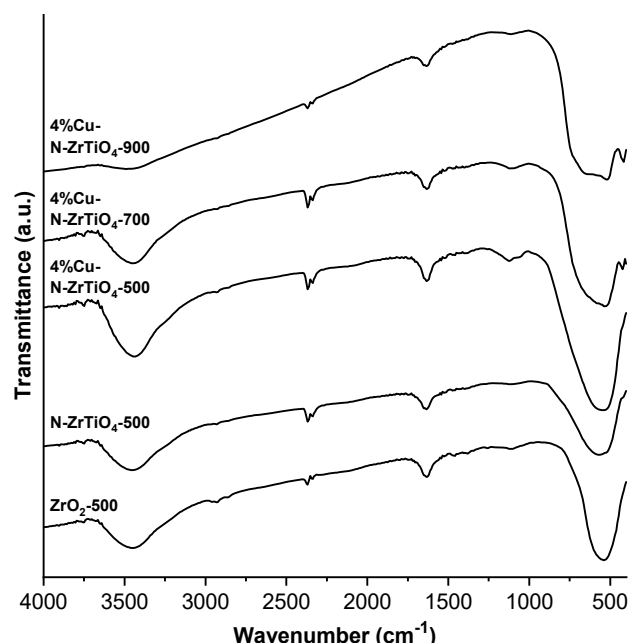
Fig 2. FTIR spectra of 4% Cu-N-ZrTiO$_4$ composites calcined at various temperatures with ZrO$_2$ and N-doped ZrTiO$_4$ as references

calcination temperature reduces the water content so that the O–H vibration frequency in the material decreases [6]. On the contrary, Ti–O–Cu vibration at 1120 cm^{-1} decreases as calcination temperature increases up to 700 °C and disappears at 900 °C. The high calcination temperature causes the sintering of metal dopants [9].

Diffraction patterns of Cu-N-ZrTiO$_4$ with ZrO$_2$, TiO$_2$, ZrTiO$_4$, and N-doped ZrTiO$_4$ as references are shown in Fig. 3. The diffraction patterns of ZrO$_2$ and TiO$_2$ calcined at 500 °C display the presence of tetragonal and anatase phases, respectively. The characteristic peaks of ZrO$_2$ tetragonal (JCPDS: 01-088-2390) appeared at 2θ = 31° (d$_{101}$) and 51° (d$_{111}$). The characteristic peaks of TiO$_2$ anatase (JCPDS: 01-084-1286) appeared at 2θ = 25° (d$_{101}$) and 48° (d$_{200}$). No Cu or CuO patterns were observed, even at 10% Cu-N-ZrTiO$_4$.

The diffraction pattern of Cu-N-ZrTiO$_4$ calcined at 500 °C has a characteristic low-intensity anatase peak at 25° (d$_{101}$). The presence of copper and nitrogen dopants inhibits the crystallization of anatase [13], while presence of Zr^{4+} in the TiO$_2$ system also inhibits the transformation of anatase to rutile [14]. The diffraction
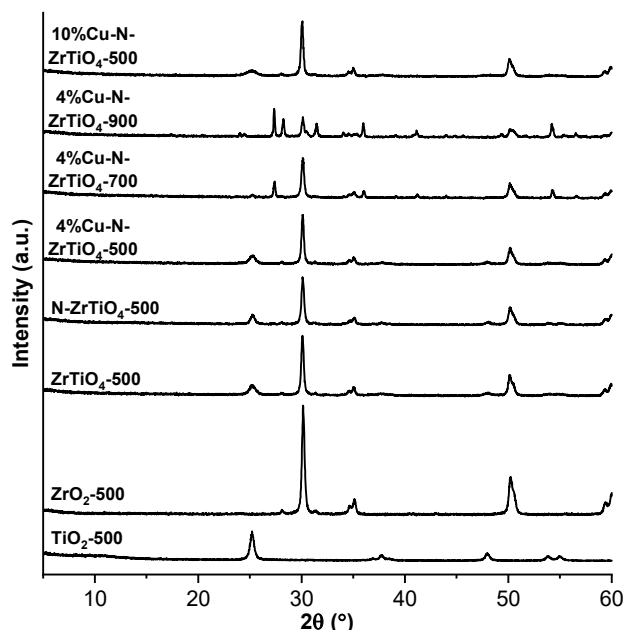
Fig 3. X-ray diffraction patterns of various Cu-N-ZrTiO$_4$ and references

pattern of ZrTiO$_4$ showed significant changes after calcination at higher temperatures. The diffraction pattern of 4% Cu-N-ZrTiO$_4$ composite after calcination at 700 °C showed rutile characteristics at 2θ = 27.5° (d$_{110}$) and 36.1° (d$_{101}$), while the anatase peak at 2θ = 25° (d$_{101}$) disappeared. Moreover, the diffraction pattern of 4% Cu-N-ZrTiO$_4$ after calcination at 900 °C exhibits an intense rutile pattern (JCPDS: 01-076-1938) at 2θ = at 27° (d$_{110}$), 36° (d$_{101}$), 41° (d$_{111}$) and 54° (d$_{211}$), while the tetragonal phase transforms to monoclinic (JCPDS: 01-088-2390), displaying a pattern at 2θ = 28° (d$_{-111}$), 31° (d$_{111}$), 34° (d$_{002}$) and 51° (d$_{220}$).

The average crystallite size of Cu-N-ZrTiO$_4$, particularly anatase and rutile, at various Cu concentrations and calcination temperatures has been shown in Table 2. The d$_{101}$ reflex of the anatase phase and the d$_{110}$ reflex of the rutile phase were chosen to calculate the crystallite size [15]. The crystallite size of the tetragonal phase shows no difference among Cu-N-ZrTiO$_4$, except 4% Cu-N-ZrTiO$_4$ after calcination at 900 °C displays a monoclinic phase. The lower anatase crystallite size of all Cu-N-ZrTiO$_4$ compared to that of pristine TiO$_2$ indicates the inhibition of anatase crystallization by copper, which is doped properly in the structure of ZrTiO$_4$.

SEM-EDX images of ZrO$_2$ and 4% Cu-N-ZrTiO$_4$ calcined at 500 °C are shown in Fig. 4. The morphology of 4% Cu-N-ZrTiO$_4$ appears slightly rougher than the ZrO$_2$ reference, while the particle size distribution of Cu-N-ZrTiO$_4$ is larger than ZrO$_2$.

The surface elemental compositions of ZrO$_2$ and 4% Cu-N-ZrTiO$_4$ based on SEM images in Fig. 4 are presented in Table 3. The mass percentage of Zr is greater than Ti because Zr is a supporting material, so it will be more dominant [16]. The low amount of detected copper indicates that the Cu dopant was doped on the ZrTiO$_4$ surface [23].

SRUV-Vis spectra of Cu-N-ZrTiO$_4$ with various copper concentrations and calcination temperatures are shown in Fig. 5(a). The inflection point (absorption edge) of each synthesized photocatalyst is already at a wavelength of greater than 400 nm. This is due to the

Table 2. The average crystallite size of various Cu-N-ZrTiO$_4$

Material	Crystal phase	L (nm)
TiO$_2$ 500 °C	Anatase	49
ZrTiO$_4$ 500 °C	Anatase	46
N-doped ZrTiO$_4$ 500 °C	Anatase	38
2% Cu-N-ZrTiO$_4$ 500 °C	Anatase	36
4% Cu-N-ZrTiO$_4$ 500 °C	Anatase	34
4% Cu-N-ZrTiO$_4$ 700 °C	Anatase	45
	Rutile	48
4% Cu-N-ZrTiO$_4$ 900 °C	Rutile	50
6% Cu-N-ZrTiO$_4$ 500 °C	Anatase	35
8% Cu-N-ZrTiO$_4$ 500 °C	Anatase	36
10% Cu-N-ZrTiO$_4$ 500 °C	Anatase	37
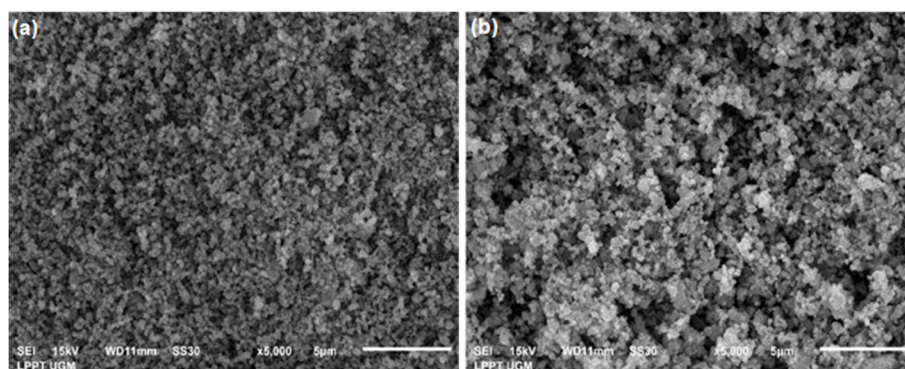
Fig 4. SEM images of (a) ZrO_2 and (b) 4% Cu-N-ZrTiO$_4$ calcined at 500 °C

Table 3. EDX analysis of ZrO_2 and 4% Cu-N-ZrTiO$_4$ calcined at 500 °C

Material	% Mass				
	Zr	O	Ti	N	Cu
ZrO_2	60.46	39.54	-	-	-
4% Cu-N-ZrTiO$_4$ 500 °C	30.76	38.92	23.96	3.93	2.43
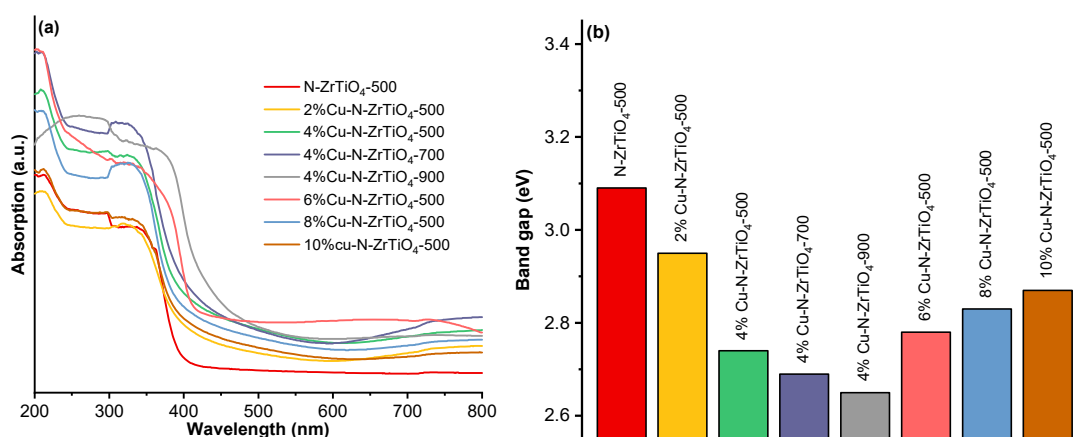
Fig 5. (a) UV-Vis absorption spectra and (b) calculated band gap of various Cu-N-ZrTiO$_4$

heterojunction between the valence band and conduction band of ZrO_2 with TiO_2 [24]. The wide bandgap (E_g) of ZrO_2 mixes with the relatively small Eg of TiO_2 until it reaches equilibrium, resulting in a ZrTiO$_4$ band gap with a slightly smaller Eg [27]. Codoping of both nitrogen and copper shifts the absorption edge of the ZrTiO$_4$ composite towards the visible light region until it reaches the saturation point [31]. If the injected dopants have reached the saturation point, the doping effect is reduced [28]. The addition of Cu and N dopants succeeded in shifting the absorption band towards a longer wavelength from 401.29 to 467.92 nm, which is in the visible-light region.

The E_g of the synthesized material is presented in Fig. 5(b). The addition of Cu and N dopants into ZrTiO$_4$ material reduces the Eg from 3.09 to the lowest 2.65 eV. The band gap decreases until reaching 4% of Cu co-doping, then increases with the increasing Cu concentration. Excess Cu concentrations above 4% can form aggregates and are not evenly distributed in the composite [29]. The absorption edges of 4% Cu-N-ZrTiO$_4$ calcined at 700 and 900 °C are shifted to the visible light region, thus resulting low Eg (2.69 and 2.65 eV, respectively). The calcination temperature above 500 °C causes the synthesized material to undergo
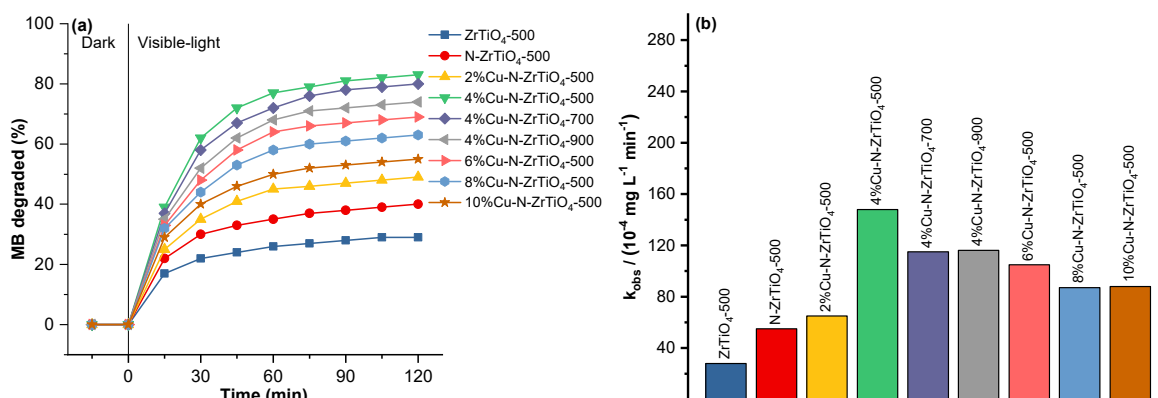
Fig 6. (a) Photo-degradation of MB over time and (b) observed rate constants of various Cu-N-ZrTiO$_4$ within 60 min irradiation

a phase transformation from anatase to rutile, which exhibits a lower Eg [14].

The photocatalytic activity of Cu-N-ZrTiO$_4$ was evaluated by applying the composite to the degradation of MB in the dark and visible light using a LIFE MAX 30W/765 PHILIPS TLD lamp. The percentage of MB degraded is shown in Fig. 6(a). In the dark, the percentage was very small (under 5%) because there was no photon to generate •OH radicals [30]. Under the exposure of light, the degradation percentages increased because the photon stimulates the photocatalyst to generate •OH radicals from water molecules [31]. When the photocatalyst is irradiated with high energy, it will produce holes (h$^+$) that are strong oxidizing agents to form •OH radicals, and these radicals degrade MB into simpler compounds [34].

Based on Fig. 6(a), there was a significant increase in the percentage of degradation at 15–60 min, while the increase in degradation at 75–120 min was less significant. Fig. 6(b) presents the observed rate constants of various Cu-N-ZrTiO$_4$ from a pseudo-first-order kinetics model [36]. The photocatalytic activity of all Cu-N-ZrTiO$_4$ is higher than references, i.e., pristine ZrTiO$_4$ and N-doped ZrTiO$_4$. The co-doping of Cu improves the photocatalytic activity of N-doped ZrTiO$_4$ [23]. The 4% Cu-N-ZrTiO$_4$ composite calcined at 500 °C has the highest photocatalytic activity, while 2% Cu-N-ZrTiO$_4$ calcined at 500 °C has the lowest photocatalytic activity. The increasing amount of Cu above 4% decreases the photocatalytic activity of the composite due to diminishing doping effect by the saturation of Cu co-

doping. The increasing calcination temperature above 500 °C also decreases photocatalytic activity of the composite due to the formation of rutile phase.

■ CONCLUSION

Copper-and-nitrogen-codoped ZrTiO$_4$ photocatalyst (Cu-N-ZrTiO$_4$) has been successfully prepared through the sol-gel process. FTIR analysis shows that there is an absorption band at 1200 cm^{-1} which relates to the Ti–O–Cu vibration as it intensifies at 4% of copper concentration. Co-doping with nitrogen and copper, as well as coupling with ZrO$_2$, influence the crystallization of anatase and rutile at a higher temperature. The absorption band is also shifted towards a longer wavelength from 401.29 to 467.92 nm, which is responsive to visible light. Cu-N-ZrTiO$_4$ photocatalyst can degrade 4 mg L^{-1} MB solution up to 83% at 120 min of irradiation time. Cu and N co-dopants give synergistic effects in improving the photocatalytic activity of ZrTiO$_4$, and it is proven to have potential as a photocatalyst to decompose dyes under visible light irradiation. Further studies regarding the photocatalyst stability of the composite are necessary to be conducted.

■ REFERENCES

[1] Al-Mamun, M.R., Kader, S., Islam, M.S., and Khan, M.Z.H., 2019, Photocatalytic activity improvement and application of UV-TiO$_2$ photocatalysis in textile wastewater treatment: A review, *J. Environ. Chem. Eng.*, 7 (5), 103248.

[2] Hamdy, M.S., Saputera, W.H., Groenen, E.J., and Mul, G., 2014, A novel TiO₂ composite for photocatalytic wastewater treatment, *J. Catal.*, 310, 75–83.

[3] Zhang, T., Xiang, Y., Su, Y., Zhang, Y., Huang, X., and Qian, X., 2022, Anchoring of copper sulfide on cellulose fibers with polydopamine for efficient and recyclable photocatalytic degradation of organic dyes, *Ind. Crops Prod.*, 187, 115357.

[4] Yan, K., Wu, G., Jarvis, C., Wen, J., and Chen, A., 2014, Facile synthesis of porous microspheres composed of TiO₂ nanorods with high photocatalytic activity for hydrogen production, *Appl. Catal. Environ.*, 148-149, 281–287.

[5] Yaacob, N., Sean, G.P., Nazri, N.A.M., Ismail, A.F., Zainol Abidin, M.N., and Subramaniam, M.N., 2021, Simultaneous oily wastewater adsorption and photo-degradation by ZrO₂–TiO₂ heterojunction photocatalysts, *J. Water Process Eng.*, 39, 101644.

[6] El-Sharkawy, E., Soliman, A.Y., and Al-Amer, K.M., 2007, Comparative study for the removal of methylene blue via adsorption and photocatalytic degradation, *J. Colloid Interface Sci.*, 310 (2), 498–508.

[7] Chen, D., Jiang, Z., Geng, J., Wang, Q., and Yang, D., 2017, Carbon and nitrogen co-doped TiO₂ with enhanced visible-light photocatalytic activity, *Ind. Eng. Chem. Res.*, 46 (9), 2741–2746.

[8] Liu, W.J., Zeng, F.X., Jiang, H., Zhang, X.S., and Li, W.W., 2012, Composite Fe₂O₃ and ZrO₂/Al₂O₃ photocatalyst: Preparation, characterization, and studies on the photocatalytic and chemical stability, *Chem. Eng. J.*, 180, 9–18.

[9] Sharma, A., and Dutta, R.K., 2010, Studies on drastic improvement of photocatalytic degradation of acid orange-74 dye by TPPO capped CuO nanoparticles with suitable electron capturing agents, *RSC Adv.*, 5 (54), 43815–43823.

[10] Jing, Y., Yin, H., Li, C., Chen, J., Wu, S., Liu, H., Xie, L., Lei, Q., Sun, M., and Yu, S., 2022, Fabrication of Pt doped TiO₂-ZnO@ZIF-8 core@shell photocatalyst with enhanced activity for phenol degradation, *Environ. Res.*, 203, 111819.

[11] Verma, S., Rani, S., Kumar, S., dan Khan, M.A.M., 2018, Rietveld refinement, micro-structural, optical and thermal parameters of zirconium titanate composites, *Ceram. Int.*, 44 (2), 1653–1661.

[12] Liang, Q., Liu, X., Zeng, G., Liu, Z., Tang, L., Shao, B., Zeng, Z., Zhang, W., Liu, Y., Cheng, M., Tang, W., and Gong, S., 2019, Surfactant-assisted synthesis of photocatalysts: Mechanism, synthesis, *Chem. Eng. J.*, 372, 429–451.

[13] Mogal, S.I., Mishra, M., Gandhi, V.G., and Tayade, R.J., 2012, Metal doped titanium dioxide: Synthesis and effect of metal ions on physico-chemical and photocatalytic properties, *Mater. Sci. Forum*, 734, 364–378.

[14] Wang, J., Zhao, Y.F., Wang, T., Li, H., and Li, C., 2015, Photonic, and photocatalytic behavior of TiO₂ mediated by Fe, CO, Ni, N doping and co-doping, *Phys. B*, 478, 6–11.

[15] Allen, N.S., Mahdjoub, N., Vishnyakov, V., Kelly, P.J., and Kriek, R.J., 2018, The effect of crystalline phase (anatase, brookite and rutile) and size on the photocatalytic activity of calcined polymorphic titanium dioxide (TiO₂), *Polym. Degrad. Stab.*, 150, 31–36.

[16] Zhang, J., Zhou, P., Liu, J., and Yu, J., 2014, New understanding of the difference of photocatalytic activity among anatase, rutile and brookite TiO₂, *Phys. Chem. Chem. Phys.*, 16 (38), 20382–20386.

[17] Gnanaprakasam, A., Sivakumar, V.M., and Thirumarimurugan, M., 2015, Influencing parameters in the photocatalytic degradation of organic effluent via nanometal oxide catalyst: A review, *Indian J. Mater. Sci.*, 2015, 601827.

[18] Barkul, R.P., Koli, V.B., Shewale, V.B., Patil, M.K., and Delekar, S.D., 2016, Visible active nanocrystalline N-doped anatase TiO₂ particles for photocatalytic mineralization studies, *Mater. Chem. Phys.*, 173, 42–51.

[19] Shao, G.N., Imran, S.M., Jeon, S.J., Engole, M., Abbas, N., Salman Haider, M., Kang, S.J., and Kim, H.T., 2014, Sol-gel synthesis of photoactive zirconia-titania from metal salts and investigation of their photocatalytic properties in the photo-degradation of methylene blue, *Powder Technol.*, 258, 99–109.

[20] Zheng, J., Sun, L., Jiao, C., Shao, Q., Lin, J., Pan, D., Naik, N., and Guo, Z., 2021, Hydrothermally synthesized Ti/Zr bimetallic MOFs derived N self-doped TiO_2/ZrO_2 composite catalysts with enhanced photocatalytic degradation of methylene blue, *Colloids Surf., A*, 623, 126629.

[21] Sherly, E.D., Vijaya, J.J., Selvam, N.C.S., and Kennedy, L.J., 2014, Microwave assisted combustion synthesis of coupled $ZnO-ZrO_2$ nanoparticles and their role in the photocatalytic degradation of 2,4-dichlorophenol, *Ceram. Int.*, 40 (4), 5681–5691.

[22] French, R.H., Glass, S.J., Ohuchi, F.S., Xu, Y.N., and Ching, W.Y., 1994, Experimental and theoretical determination of the electronic structure and optical properties of three phases of ZrO_2, *Phys. Rev. B: Condens. Matter Mater. Phys.*, 49 (8), 5133–5142.

[23] Piątkowska, A., Janus, M., Szymański, K., and Mozia, S., 2021, C-, N- and S-doped TiO_2 photocatalysts: A review, *Catalysts*, 11 (1), 144.

[24] Kumaresan, L., Prabhu, A., Palanichamy, M., Arumugam, E., and Murugesan, V., 2014, Synthesis and characterization of Zr^{4+}, La^{3+} and Ce^{3+} doped mesoporous TiO_2: Evaluation of their photocatalytic activity, *J. Hazard. Mater.*, 186 (2-3), 1183–1192.

[25] Dutta, H., Nandy, A., and Pradhan, S.K., 2016, Microstructure and optical characterizations of mechanosynthesized nanocrystalline semiconducting $ZrTiO_4$ compound, *J. Phys. Chem. Solids*, 95, 56–64.

[26] Hayati, R., Kurniawan, R., Prasetyo, N., Sudiono, S., and Syoufian, A., 2022, Codoping effect of nitrogen (N) to iron (Fe) doped zirconium titanate ($ZrTiO_4$) composite toward its visible light responsiveness as photocatalysts, *Indones. J. Chem.*, 22 (3), 692–702.

[27] Muslim, M.I., Kurniawan, R., Pradipta, M.F., Trisunaryanti, W., and Syoufian, A., 2021, The effects of manganese dopant content and calcination temperature on properties of titania-zirconia composite, *Indones. J. Chem.*, 21 (4), 882–890.

[28] Alifi, A., Kurniawan, R., and Syoufian, A., 2020, Zinc-doped titania embedded on the surface of Zirconia: A potential visible-responsive photocatalyst material, *Indones, J. Chem.*, 20 (6), 1374–1381.

[29] Kim, J.Y., Kim, C.S., Chang, H.K., and Kim, T.O., 2011, Synthesis and characterization of N doped TiO_2/ZrO_2 visible light photocatalysts, *Adv. Powder Technol.*, 22 (3), 443–448.

[30] Venkatesan, A., Al-onazi, W.A., Elshikh, M.S., Pham, T.H., Suganya, S., Boobas, S., and Priyadharsan, A., 2022, Study of synergistic effect of cobalt and carbon codoped TiO_2 photocatalyst for visible light induced degradation of phenol, *Chemosphere*, 305, 135333.

[31] Kim, C.S., Shin, J.W., Cho, Y.H., Jang, H.D., Byun, H.S., and Kim, T.O., 2013, Synthesis and characterization of Cu/N-doped mesoporous TiO_2 visible light photocatalysts, *Appl. Catal., A*, 455, 211–218.

[32] Li, D., Qin, Q., Duan, X., Yang, J., Guo, W., and Zheng, W., 2013, General one-pot template-free hydrothermal method to metal oxide hollow spheres and their photocatalytic activities and lithium storage properties, *ACS Appl. Mater. Interfaces*, 5 (18), 9095–9100.

[33] Khan, S., Kim, J., Sotto, A., and van der Bruggen, B., 2015, Humic acid fouling in a submerged photocatalytic membrane reactor with binary TiO_2-ZrO_2 particles, *J. Ind. Eng. Chem.*, 21, 779–786.

[34] Singh, H., Sunaina, S., Yadav, K.K., Bajpai, V.K., and Jha, M., 2020, Tuning the bandgap of m-ZrO_2 by incorporation of copper nanoparticles into visible region for the treatment of organic pollutants, *Mater. Res. Bull.*, 123, 110698.

[35] Kurniawan, R., Sudiono, S., Trisunaryanti, W., and Syoufian, A., 2019, Synthesis of iron-doped zirconium titanate as a potential visible-light responsive photocatalyst, *Indones. J. Chem.*, 19 (2), 454–460.

[36] Syoufian, A., and Nakashima, K., 2008, Degradation of methylene blue in aqueous dispersion of hollow titania photocatalyst: Study of reaction enhancement by various electron scavengers, *J. Colloid Interface Sci.*, 317 (2), 507–512.